Geometrically exact analysis of shells with an exact initial geometry by a meshless method

Carlos Tiago
Instituto Superior Técnico, Universidade Técnica de Lisboa, Lisboa – Portugal
Paulo M. Pimenta
Escola Politécnica, Universidade de São Paulo, SP – Brazil

Abstract

The applicability of a meshfree approximation method, namely the EFG method, on fully geometrically exact analysis of shells is investigated. Based on a unified nonlinear theory of shells, which allows for arbitrarily large rotations and displacements, a Galerkin approximation with MLS functions is settled. A hybrid method of analysis is proposed where the solution is obtained by the approximation of the generalized internal displacement fields and the generalized boundary tractions.

An extension of the arc-length method that includes the generalized internal displacement fields, the generalized boundary tractions and the load parameter in the constraint equation of the hyperellipsis is proposed to solve the resulting nonlinear problem. A consistent linearization procedure is performed, resulting a semi-definite system matrix which, for hyperelastic materials and conservative loadings, is always symmetric (even for configurations far from the generalized equilibrium trajectory).

Differently from the standard Finite Element Methods (FEM), the resulting solution are (arbitrary) smooth generalized displacements and stress fields. Also, the representation of the initial configuration is geometrically exact, contrary the usual FEM, where a C^0 approximation of the original problem is made.

Keywords: shells, geometrically exact, exact initial geometry, meshfree, hyperelastic material, hybrid weak form.

1 Introduction

1.1 Historical background

The research on geometrically exact shell models was initiated by Simo and co-workers. The formulation and parametrization of the model was presented in [1], where the hypothesis of *one inextensible director*, used in the present work, was already considered. In the subsequent papers the linear and nonlinear computational aspects of the theory are dealt. Other perspectives were latter considered,

Mechanics of Solids in Brazil 2007, Marcílio Alves & H.S. da Costa Mattos (Editors)
Brazilian Society of Mechanical Sciences and Engineering, ISBN 978-85-85769-30-7

like through-the-thickness stretch, plasticity constitutive model, time-stepping conserving algorithms for dynamical analysis and shell intersections problems.

Nevertheless, some drawbacks were still present like the need for complex configuration updates and the use of *assumed strain* methods to avoid the *shear locking* effect.

On the *twin* papers [2, 3] a unified theory for beams and shells, respectively, was presented. Here, the fundamental variable for parameterizing the rotation tensor is the rotation vector, delivering an expression for the tangent stiffness which is always symmetric[1] even far from the equilibrium path.

Implementation of this theory for beams was presented in [4], which was latter generalized to curved rods [5] and to accommodate warping and a genuine finite strain constitutive relation [6].

In the shell model implementation of [7] a constitutive relation was derived based on a true plane stress condition. The generalization presented in [8] accommodates the thickness variation of the shell, thus allowing the use of a full three dimensional finite strain constitutive model.

The traditional version of the Finite Element Method[2] (FEM) is, invariably, the chosen numerical tool to discretize the unknown fields. However, some of the inconveniences of the FEM can be overcome by the use of meshfree discretizations, like (i) the need to explicitly set up incidences relations between nodes (in order to shape elements) and (ii) the lack of equilibrium between adjacent elements. Meshfree methods are nowadays a well establish tool to solve engineering problems. For reviews see, *e. g.*, [9].

The first geometrically exact analysis using meshfree approximations was presented in [10] for rods. Latter, this work was generalized for shell analysis in [11].

1.2 Scope of the present work

In the present work an alternative method for the solution of shell is presented. Hence, a fresh approximation method is applied to the numerical solution of a, also recent, shell model.

In the FEM context the use of a initial curved elements is not imperative, as established in [12]. This behaviour can be explained by combining two sorts of reasons. On one hand, in the FEM the *geometry* is described by the elements and, on the other hand, in shell analysis *refined meshes* are usually required. Thus, the use of assembly of flat elements to model shells is usually acceptable.

Unlike the FEM, in weak form based meshfree projections the whole shell is a *unique* domain[3], hence the consideration of initial curved geometries is essential.

A crucial enhancement in the geometrically exact shell formulation for the present work was the consideration on initially curved shells [13]. Although developed and implemented in a FEM framework, the results can be straightforwardly incorporated in the present formulation. The consideration of possibly curved shells is performed by a simple mapping from the *plane* reference configuration to the *initial* form. All the computations are done over the plane reference configuration. The theoretical

[1] For hyperelastic materials and conservative loads, of course.

[2] By traditional version of the Finite Element Method we refer to the well known displacement model using nodal shape functions for approximation both the geometry and the generalized displacements fields and imposition of the essential boundary conditions through collocation. Non–conventional formulations (like hybrid, mixed or equilibrium) are not included here.

[3] Subdivisions are possible but not advisable, as the nature of the approximation is element free.

Mechanics of Solids in Brazil 2007, Marcílio Alves & H.S. da Costa Mattos (Editors)
Brazilian Society of Mechanical Sciences and Engineering, ISBN 978-85-85769-30-7

formulation presented in those works supplies a perfect background for the development of a meshfree formulation.

In order to circumvent the non-interpolation character of the approximations, which impairs the use of collocation for imposing the boundary conditions[4], a hybrid weak form suitable for meshless approximations is presented, which includes the internal virtual work, the external virtual work and the external complementary virtual work arising from the kinematic boundary.

The exact parametrization of the rotation tensor is made through the Euler-Rodrigues formula. As *all* vectorial parameterizations of the rotation tensor, this closed-form solution has a limited range of application beyond which a singularity occurs. For circumvent this problem, an update lagrangian formulation can be used, as in [10]. However, is not common to face this problem in shell analysis.

The only kinematical assumption is the plane section hypothesis of Reissner-Mindlin. The inextensibility of the director is complemented by a plane stress condition. This is imposed over the the constitutive model, which is the neo-Hookean material.

The internal virtual work is expressed by the first Piola-Kirchhoff stress tensor and the deformation gradient.

1.3 Notation and text organization

Throughout the text italic Latin or Greek lowercase letters $(a, b, \ldots \alpha, \beta, \ldots)$ denote scalar quantities, bold italic Latin or Greek lowercase letters $(\boldsymbol{a}, \boldsymbol{b}, \ldots \boldsymbol{\alpha}, \boldsymbol{\beta}, \ldots)$ denote vectors, bold italic Latin or Greek capital letters $(\boldsymbol{A}, \boldsymbol{B}, \ldots)$ denote second-order tensors and bold blackboard italic Latin capital letters $(\mathbb{A}, \mathbb{B}, \ldots)$ denote forth-order tensors in a three dimensional Euclidian space. The same letter is used to identify the skew-symmetric second order tensors $(\boldsymbol{A}, \boldsymbol{B}, \ldots \boldsymbol{\Omega}, \boldsymbol{\Theta}, \ldots)$ and their associated axial vector $(\boldsymbol{a}, \boldsymbol{b}, \ldots \boldsymbol{\omega}, \boldsymbol{\theta}, \ldots)$.

The problem is presented in section 2. In section 3 the mappings of the initial configuration and the generalized displacements fields are introduced and the deformation and velocity gradients derived. The generalized stresses, the internal power and the external power are presented in section 4, followed by the proposed variational formulation of the problem in section 5. The suggested meshfree method and associated implementation issues are exhibited in sections 6 and 7. A numerical example is presented in section 8.

2 The model problem

Consider the shell exhibited in figure 1, where three orthonormal right-handed coordinate systems are represented, namely, $\boldsymbol{e}_i^r$ for the reference configuration, $\boldsymbol{e}_i^{\circ}$ for the initial configuration and $\boldsymbol{e}_i$ for the current configuration. The reference plane is denoted by $\Omega^r \subset \mathbb{R}^2$. The contour of Ω^r is denoted by Γ^r, *i. e.*, $\Gamma^r = \partial\Omega^r$ and can be decomposed as $\Gamma_t^r \cup \Gamma_u^r = \Gamma^r$ and $\Gamma_t^r \cap \Gamma_u^r = \emptyset$, where Γ_t^r and Γ_u^r identify the static and kinematic boundaries. The volume is identified by V^r and $H^r = [-h_b^r, h_t^r]$ is the shell thickness, both on the reference configuration. The endpoints of H^r are collected in the set

[4]In fact, with an appropriate change of coordinates this could also be archived, see [9].

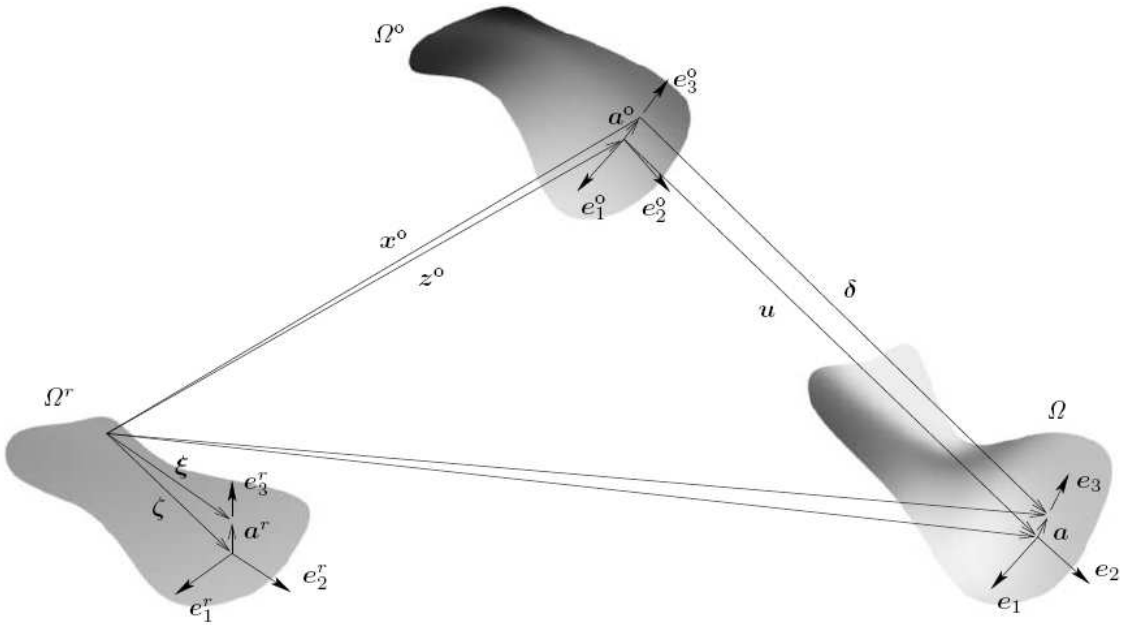

Figure 1: The reference, initial and current configurations of the shell.

$C^r = \{-h_b^r, h_t^r\}$, thus $C^r = \partial H^r$.

The reference configuration can be described by $\boldsymbol{\xi}$, which can be written as

$$\boldsymbol{\xi} = \boldsymbol{\zeta} + \boldsymbol{a}^r, \tag{1}$$

where $\boldsymbol{\zeta} = \xi_\alpha \boldsymbol{e}_\alpha^r$ defines the position of a material point over the middle plane of the reference configuration, Ω^r, and $\boldsymbol{a}^r = \zeta \boldsymbol{e}_3^r$ represents the component along the normal.

The position of the material points in the initial configuration, Ω^o, is

$$\boldsymbol{x}^o = \boldsymbol{z}^o + \boldsymbol{a}^o, \tag{2}$$

where the middle surface, $\boldsymbol{z}^o$, of the initial configuration $\Omega^o \in \mathbb{R}^3$ is defined by

$$\boldsymbol{z}^o = \boldsymbol{z}^o(\boldsymbol{\zeta}), \tag{3}$$

and the normal vector to the initial configuration is given by

$$\boldsymbol{a}^o = \boldsymbol{Q}^o \boldsymbol{a}^r, \tag{4}$$

where $\boldsymbol{Q}^o$ is the initial rotation tensor.

We assume the applied load vary linearly with a parameter, λ. Nevertheless, for simplicity, this dependance will be omitted in the following. The shell is under the action of a body forces, $\overline{\boldsymbol{b}}^{\mathrm{o}}$, per unit volume of the initial configuration and traction forces, $\overline{\boldsymbol{t}}^{\mathrm{o}}$, per unit area of the initial configuration on the top and bottom surfaces. Eventually, configuration dependant loads may be included. In the lateral surfaces the shell is subjected either prescribed tractions, per unit area of the initial configuration, or imposed displacements. Due to the kinematical assumption, the displacements of a given point, $\boldsymbol{\zeta}$, on the lateral surface are not independent along ζ.

3 Kinematics

3.1 The initial configuration

The initial rotation tensor is given by

$$\boldsymbol{Q}^{\mathrm{o}} = \boldsymbol{e}_i^{\mathrm{o}} \otimes \boldsymbol{e}_i^r. \tag{5}$$

The basis $\boldsymbol{e}_i^{\mathrm{o}}$ can be obtained by

$$\boldsymbol{e}_1^{\mathrm{o}} = \frac{\boldsymbol{z}_{,1}^{\mathrm{o}}}{\|\boldsymbol{z}_{,1}^{\mathrm{o}}\|}, \tag{6a}$$

$$\boldsymbol{e}_3^{\mathrm{o}} = \frac{\boldsymbol{z}_{,1}^{\mathrm{o}} \times \boldsymbol{z}_{,2}^{\mathrm{o}}}{\|\boldsymbol{z}_{,1}^{\mathrm{o}} \times \boldsymbol{z}_{,2}^{\mathrm{o}}\|}, \tag{6b}$$

$$\boldsymbol{e}_2^{\mathrm{o}} = \boldsymbol{e}_3^{\mathrm{o}} \times \boldsymbol{e}_1^{\mathrm{o}}. \tag{6c}$$

3.2 Initial deformation gradient

The initial deformation gradient, $\boldsymbol{F}^{\mathrm{o}}$, is given by

$$\boldsymbol{F}^{\mathrm{o}} = \frac{\partial \boldsymbol{x}^{\mathrm{o}}}{\partial \boldsymbol{\xi}_\alpha} \otimes \boldsymbol{e}_\alpha^r + \frac{\partial \boldsymbol{x}^{\mathrm{o}}}{\partial \boldsymbol{\zeta}} \otimes \boldsymbol{e}_3^r = (\boldsymbol{\eta}_\alpha^{\mathrm{o}} + \boldsymbol{K}_\alpha^{\mathrm{o}} \boldsymbol{a}^{\mathrm{o}}) \otimes \boldsymbol{e}_\alpha^r + \boldsymbol{Q}^{\mathrm{o}} \tag{7}$$

where it was introduced the vector

$$\boldsymbol{\eta}_\alpha^{\mathrm{o}} = \boldsymbol{z}_{,\alpha}^{\mathrm{o}} - \boldsymbol{Q}^{\mathrm{o}} \boldsymbol{e}_\alpha^r \tag{8}$$

and the skew-symmetric tensor

$$\boldsymbol{K}_\alpha^{\mathrm{o}} = \boldsymbol{Q}_{,\alpha}^{\mathrm{o}} \boldsymbol{Q}^{\mathrm{o}T} \tag{9}$$

whose axial vector, $\boldsymbol{\kappa}_\alpha^{\mathrm{o}}$, is given by

$$\boldsymbol{\kappa}_\alpha^{\mathrm{o}} = \mathrm{Axial}\,(\boldsymbol{K}_\alpha^{\mathrm{o}}) = \left(\boldsymbol{e}_{2,\alpha}^{\mathrm{o}} \cdot \boldsymbol{e}_3^{\mathrm{o}}\right) \boldsymbol{e}_1^{\mathrm{o}} + \left(\boldsymbol{e}_{3,\alpha}^{\mathrm{o}} \cdot \boldsymbol{e}_1^{\mathrm{o}}\right) \boldsymbol{e}_2^{\mathrm{o}} + \left(\boldsymbol{e}_{1,\alpha}^{\mathrm{o}} \cdot \boldsymbol{e}_2^{\mathrm{o}}\right) \boldsymbol{e}_3^{\mathrm{o}}. \tag{10}$$

Defining the initial strain vector as

$$\boldsymbol{\gamma}_\alpha^{\mathrm{o}} = \boldsymbol{\eta}_\alpha^{\mathrm{o}} + \boldsymbol{\kappa}_\alpha^{\mathrm{o}} \times \boldsymbol{a}^{\mathrm{o}}, \tag{11}$$

the initial deformation gradient can be written as

$$\boldsymbol{F}^{\mathrm{o}} = (\boldsymbol{\eta}_\alpha^{\mathrm{o}} + \boldsymbol{\kappa}_\alpha^{\mathrm{o}} \times \boldsymbol{a}^{\mathrm{o}}) \otimes \boldsymbol{e}_\alpha^r + \boldsymbol{Q}^{\mathrm{o}} = \boldsymbol{\gamma}_\alpha^{\mathrm{o}} \otimes \boldsymbol{e}_\alpha^r + \boldsymbol{Q}^{\mathrm{o}}. \tag{12}$$

Hence, the generalized strains in the reference configuration, $\boldsymbol{\eta}_{\alpha}^{\mathrm{o}r}$ and $\boldsymbol{\kappa}_{\alpha}^{\mathrm{o}r}$, are given by

$$\boldsymbol{\eta}_{\alpha}^{\mathrm{o}r} = \boldsymbol{Q}^{\mathrm{o}T}\boldsymbol{\eta}_{\alpha}^{\mathrm{o}} = \boldsymbol{Q}^{\mathrm{o}T}\boldsymbol{z}_{,\alpha}^{\mathrm{o}} - \boldsymbol{e}_{\alpha}^{r}, \tag{13a}$$

$$\boldsymbol{\kappa}_{\alpha}^{\mathrm{o}r} = \boldsymbol{Q}^{\mathrm{o}T}\boldsymbol{\kappa}_{\alpha}^{\mathrm{o}} = \left(\boldsymbol{e}_{2,\alpha}^{\mathrm{o}} \cdot \boldsymbol{e}_{3}^{\mathrm{o}}\right)\boldsymbol{e}_{1}^{r} + \left(\boldsymbol{e}_{3,\alpha}^{\mathrm{o}} \cdot \boldsymbol{e}_{1}^{\mathrm{o}}\right)\boldsymbol{e}_{2}^{r} + \left(\boldsymbol{e}_{1,\alpha}^{\mathrm{o}} \cdot \boldsymbol{e}_{2}^{\mathrm{o}}\right)\boldsymbol{e}_{3}^{r}. \tag{13b}$$

It is now possible to define the vector $\boldsymbol{\gamma}_{\alpha}^{\mathrm{o}r}$ through

$$\boldsymbol{\gamma}_{\alpha}^{\mathrm{o}r} = \boldsymbol{\eta}_{\alpha}^{\mathrm{o}r} + \boldsymbol{\kappa}_{\alpha}^{\mathrm{o}r} \times \boldsymbol{a}^{r}. \tag{14}$$

Hence, the initial deformation gradient, as a function of the generalized back-rotated strains, assumes the form

$$\boldsymbol{F}^{\mathrm{o}} = \boldsymbol{Q}^{\mathrm{o}}\boldsymbol{F}^{\mathrm{o}r}, \tag{15}$$

where it was introduced the initial back-rotated tensor $\boldsymbol{F}^{\mathrm{o}r}$,

$$\boldsymbol{F}^{\mathrm{o}r} = \boldsymbol{I} + \boldsymbol{\gamma}_{\alpha}^{\mathrm{o}r} \otimes \boldsymbol{e}_{\alpha}^{r}. \tag{16}$$

This tensor may be rewritten as

$$\boldsymbol{F}^{\mathrm{o}r} = \boldsymbol{f}_{i}^{\mathrm{o}r} \otimes \boldsymbol{e}_{i}^{r}, \tag{17}$$

where

$$\boldsymbol{f}_{\alpha}^{\mathrm{o}r} = \boldsymbol{e}_{\alpha}^{r} + \boldsymbol{\gamma}_{\alpha}^{\mathrm{o}r}, \tag{18a}$$

$$\boldsymbol{f}_{3}^{\mathrm{o}r} = \boldsymbol{e}_{3}^{r}. \tag{18b}$$

3.3 The displacement field

From figure 1 it can be concluded that, on the deformed configuration,

$$\boldsymbol{x} = \boldsymbol{z} + \boldsymbol{a}. \tag{19}$$

But

$$\boldsymbol{z} = \boldsymbol{z}^{\mathrm{o}} + \boldsymbol{u} \tag{20}$$

and

$$\boldsymbol{a} = \boldsymbol{Q}^{\mathrm{e}}\boldsymbol{a}^{\mathrm{o}}, \tag{21}$$

where

$$\boldsymbol{Q}^{\mathrm{e}} = \boldsymbol{I} + h_1(\theta)\,\boldsymbol{\Theta} + h_2(\theta)\,\boldsymbol{\Theta}^2 \tag{22}$$

is the effective Euler-Rodrigues rotation tensor. The trigonometric functions $h_1(\theta)$ and $h_2(\theta)$ are given in, *e. g.*, [7].

Taking into account that $\boldsymbol{a}^{\mathrm{o}} = \boldsymbol{Q}^{\mathrm{o}}\boldsymbol{a}^{r}$, by rotation composition,

$$\boldsymbol{a} = \boldsymbol{Q}^{\mathrm{e}}\boldsymbol{a}^{\mathrm{o}} = \boldsymbol{Q}^{\mathrm{e}}\boldsymbol{Q}^{\mathrm{o}}\boldsymbol{a}^{r} = \boldsymbol{Q}\boldsymbol{a}^{r}, \tag{23}$$

where $\boldsymbol{Q} = \boldsymbol{Q}^{\mathrm{e}}\boldsymbol{Q}^{\mathrm{o}}$ describes the rotation from the plane reference configuration to the deformed configuration.

3.4 The total deformation gradient

The total deformation gradient, $\boldsymbol{F}$, is given by

$$\boldsymbol{F} = \frac{\partial \boldsymbol{x}}{\partial \boldsymbol{\xi}_{\alpha}} \otimes \boldsymbol{e}_{\alpha}^{r} + \frac{\partial \boldsymbol{x}}{\partial \boldsymbol{\zeta}} \otimes \boldsymbol{e}_{3}^{r} = (\boldsymbol{\eta}_{\alpha} + \boldsymbol{K}_{\alpha}\boldsymbol{a}) \otimes \boldsymbol{e}_{\alpha}^{r} + \boldsymbol{Q}, \tag{24}$$

where the skew-symmetric tensor

$$\boldsymbol{K}_{\alpha} = \boldsymbol{Q}_{,\alpha}\boldsymbol{Q}^{T} \tag{25}$$

was introduced.

The latter can be expressed as

$$\boldsymbol{K}_{\alpha} = \boldsymbol{Q}_{,\alpha}\boldsymbol{Q}^{T} = \boldsymbol{K}_{\alpha}^{\mathrm{e}} + \boldsymbol{Q}^{\mathrm{e}}\boldsymbol{K}_{\alpha}^{\mathrm{o}}\boldsymbol{Q}^{\mathrm{e}T}, \tag{26}$$

where the skew-symmetric tensors

$$\boldsymbol{K}_{\alpha}^{\mathrm{e}} = \boldsymbol{Q}_{,\alpha}^{\mathrm{e}}\boldsymbol{Q}^{\mathrm{e}T}, \tag{27}$$

$$\boldsymbol{K}_{\alpha}^{\mathrm{o}} = \boldsymbol{Q}_{,\alpha}^{\mathrm{o}}\boldsymbol{Q}^{\mathrm{o}T}, \tag{28}$$

were introduced.

The axial vector $\boldsymbol{K}_{\alpha}$ is given by

$$\boldsymbol{\kappa}_{\alpha} = \mathrm{Axial}\,(\boldsymbol{K}_{\alpha}) = \boldsymbol{\kappa}_{\alpha}^{\mathrm{e}} + \boldsymbol{Q}^{\mathrm{e}}\boldsymbol{\kappa}_{\alpha}^{\mathrm{o}}, \tag{29}$$

where

$$\boldsymbol{\kappa}_{\alpha}^{\mathrm{e}} = \mathrm{Axial}\,(\boldsymbol{K}_{\alpha}^{\mathrm{e}}) = \boldsymbol{\Gamma}\boldsymbol{\theta}_{,\alpha} \tag{30}$$

and the tensor $\boldsymbol{\Gamma}$ is defined in [7].

The generalized back-rotated strains are given by

$$\boldsymbol{\eta}_{\alpha}^{r} = \boldsymbol{Q}^{T}\boldsymbol{\eta}_{\alpha} = \boldsymbol{Q}^{T}\boldsymbol{z}_{,\alpha} - \boldsymbol{e}_{\alpha}^{r}, \tag{31a}$$

$$\boldsymbol{\kappa}_{\alpha}^{r} = \boldsymbol{Q}^{T}\boldsymbol{\kappa}_{\alpha} = \boldsymbol{\kappa}_{\alpha}^{er} + \boldsymbol{\kappa}_{\alpha}^{or}. \tag{31b}$$

An alternative form of expressing (31b) is

$$\boldsymbol{\kappa}_{\alpha}^{r} = \boldsymbol{Q}^{\mathrm{o}T}\left(\boldsymbol{\Gamma}^{T}\boldsymbol{\theta}_{,\alpha} + \boldsymbol{\kappa}_{\alpha}^{\mathrm{o}}\right). \tag{32}$$

Substituting this results in the deformation gradient expression, (24), results

$$\boldsymbol{F} = (\boldsymbol{\eta}_\alpha + \boldsymbol{K}_\alpha \boldsymbol{a}) \otimes \boldsymbol{e}_\alpha^r + \boldsymbol{Q} = \boldsymbol{Q}\left(\boldsymbol{I} + \boldsymbol{\gamma}_\alpha^r \otimes \boldsymbol{e}_\alpha^r\right), \tag{33}$$

where it was defined the vector

$$\boldsymbol{\gamma}_\alpha^r = \boldsymbol{\eta}_\alpha^r + \boldsymbol{\kappa}_\alpha^r \times \boldsymbol{a}^r. \tag{34}$$

It is still possible to write

$$\boldsymbol{F} = \boldsymbol{Q}\boldsymbol{F}^r, \tag{35}$$

where

$$\boldsymbol{F}^r = \boldsymbol{I} + \boldsymbol{\gamma}_\alpha^r \otimes \boldsymbol{e}_\alpha^r \tag{36}$$

is the total back-rotated deformation gradient.

This can be written

$$\boldsymbol{F}^r = \boldsymbol{f}_i^r \otimes \boldsymbol{e}_i^r, \tag{37}$$

where

$$\boldsymbol{f}_\alpha^r = \boldsymbol{e}_\alpha^r + \boldsymbol{\gamma}_\alpha^r, \tag{38a}$$

$$\boldsymbol{f}_3^r = \boldsymbol{e}_3^r. \tag{38b}$$

The generalized strains of the shell model can be collected in the vector

$$\boldsymbol{\varepsilon}^r = \begin{bmatrix} \boldsymbol{\varepsilon}_1 \\ \boldsymbol{\varepsilon}_2 \end{bmatrix}, \tag{39}$$

where

$$\boldsymbol{\varepsilon}_\alpha^r = \begin{bmatrix} \boldsymbol{\eta}_\alpha^r \\ \boldsymbol{\kappa}_\alpha^r \end{bmatrix} = \begin{bmatrix} \boldsymbol{Q}^T \boldsymbol{z}_\alpha - \boldsymbol{e}_\alpha^r \\ \boldsymbol{Q}^{\mathrm{o}T}\left(\boldsymbol{\Gamma}^T \boldsymbol{\theta}_{,\alpha} + \boldsymbol{\kappa}_\alpha^{\mathrm{o}}\right) \end{bmatrix}. \tag{40}$$

3.5 Effective deformation gradient

The deformation gradient can be evaluated with the aid of the chain rule of differentiation by

$$\boldsymbol{F} = \frac{\partial \boldsymbol{x}}{\partial \boldsymbol{\xi}_\alpha} = \frac{\partial \boldsymbol{x}}{\partial \boldsymbol{x}^{\mathrm{o}}} \frac{\partial \boldsymbol{x}^{\mathrm{o}}}{\partial \boldsymbol{x}} = \boldsymbol{F}^{\mathrm{e}} \boldsymbol{F}^{\mathrm{o}} \tag{41}$$

from where it can be concluded

$$\boldsymbol{F}^{\mathrm{e}} = \boldsymbol{F}\boldsymbol{F}^{\mathrm{o}-1}. \tag{42}$$

It is possible to evaluate explicitly $\boldsymbol{F}^{\mathrm{o}-1}$ by

$$\boldsymbol{F}^{\mathrm{o}-1} = \left(\boldsymbol{Q}^{\mathrm{o}} \boldsymbol{F}^{\mathrm{o}r}\right)^{-1} = \boldsymbol{F}^{\mathrm{o}r-1} \boldsymbol{Q}^{\mathrm{o}-1} = \boldsymbol{F}^{\mathrm{o}r-1} \boldsymbol{Q}^{\mathrm{o}T} = \frac{1}{J^{\mathrm{o}}} \left(\boldsymbol{e}_i^r \otimes \boldsymbol{g}_i^{\mathrm{o}r}\right) \boldsymbol{Q}^{\mathrm{o}T}, \tag{43}$$

where $J^{\mathrm{o}} = \det \boldsymbol{F}^{\mathrm{o}r}$[5], *i. e.*,

$$J^{\mathrm{o}} = \det\left(\boldsymbol{F}^{\mathrm{o}r}\right) = \det\left(\boldsymbol{f}_i^{\mathrm{o}r} \otimes \boldsymbol{e}_i^r\right) = \boldsymbol{f}_1^{\mathrm{o}r} \cdot \boldsymbol{f}_2^{\mathrm{o}r} \times \boldsymbol{f}_3^{\mathrm{o}r} \tag{44}$$

and

$$\boldsymbol{g}_1^{\mathrm{o}r} = \boldsymbol{f}_2^{\mathrm{o}r} \times \boldsymbol{f}_3^{\mathrm{o}r}, \tag{45a}$$

$$\boldsymbol{g}_2^{\mathrm{o}r} = \boldsymbol{f}_3^{\mathrm{o}r} \times \boldsymbol{f}_1^{\mathrm{o}r}, \tag{45b}$$

$$\boldsymbol{g}_3^{\mathrm{o}r} = \boldsymbol{f}_1^{\mathrm{o}r} \times \boldsymbol{f}_2^{\mathrm{o}r}. \tag{45c}$$

Using (35) and (43) in (42) gives rise to

$$\boldsymbol{F}^{\mathrm{e}} = \boldsymbol{F}\boldsymbol{F}^{\mathrm{o}-1} = \boldsymbol{Q}\left(\boldsymbol{f}_i^{\mathrm{e}r} \otimes \boldsymbol{e}_i^{\mathrm{o}}\right), \tag{46}$$

where

$$\boldsymbol{f}_3^{\mathrm{e}r} = \boldsymbol{e}_3^r, \tag{47a}$$

$$\boldsymbol{f}_\alpha^{\mathrm{e}r} = J^{\mathrm{o}-1}\boldsymbol{f}_\beta^r\left(\boldsymbol{g}_\beta^{\mathrm{o}r} \cdot \boldsymbol{e}_\alpha^r\right). \tag{47b}$$

By analogy with (18a) and (38a) the effective strain deformation vector is now introduced as

$$\boldsymbol{\gamma}_\alpha^{\mathrm{e}r} = \boldsymbol{f}_\alpha^{\mathrm{e}r} - \boldsymbol{e}_\alpha^r = J^{\mathrm{o}-1}\left(\boldsymbol{e}_\alpha^r \cdot \boldsymbol{g}_\beta^{\mathrm{o}r}\right)\left(\boldsymbol{e}_\beta^r + \boldsymbol{\gamma}_\beta^r\right) - \boldsymbol{e}_\alpha^r \tag{48}$$

3.6 Velocity gradient

The time variation of the generalized strains can be collected in a vector

$$\dot{\boldsymbol{\varepsilon}}^r = \begin{bmatrix} \dot{\boldsymbol{\varepsilon}}_1 \\ \dot{\boldsymbol{\varepsilon}}_2 \end{bmatrix}, \tag{49}$$

where

$$\dot{\boldsymbol{\varepsilon}}_\alpha^r = \begin{bmatrix} \dot{\boldsymbol{\eta}}_\alpha^r \\ \dot{\boldsymbol{\kappa}}_\alpha^r \end{bmatrix} = \begin{bmatrix} \boldsymbol{Q}^T\left(\dot{\boldsymbol{u}}_{,\alpha} + \boldsymbol{Z}_{,\alpha}\boldsymbol{\Gamma}\dot{\boldsymbol{\theta}}\right) \\ \boldsymbol{Q}^T\left(\boldsymbol{\Gamma}_{,\alpha}\dot{\boldsymbol{\theta}} + \boldsymbol{\Gamma}\dot{\boldsymbol{\theta}}_{,\alpha}\right) \end{bmatrix}. \tag{50}$$

Introducing the generalized displacements vector $\boldsymbol{d}$, given by

$$\boldsymbol{d} = \begin{bmatrix} \boldsymbol{u} \\ \boldsymbol{\theta} \end{bmatrix} \tag{51}$$

the time variation of the generalized strains can be recast in the compact form

$$\dot{\boldsymbol{\varepsilon}}^r = \boldsymbol{\Psi}\boldsymbol{\Delta}\dot{\boldsymbol{d}} \tag{52}$$

[5]The superscript r in J^{o} was suppressed because $\det\left(\boldsymbol{F}^{\mathrm{o}}\right) = \det\left(\boldsymbol{F}^{\mathrm{o}r}\right)$ and, therefore, $J^{\mathrm{o}} = J^{\mathrm{o}r}$.

where

$$\boldsymbol{\Psi} = \begin{bmatrix} \boldsymbol{Q}^T & \boldsymbol{O} & \boldsymbol{O} & \boldsymbol{O} & \boldsymbol{Q}^T\boldsymbol{Z}_{,1}\boldsymbol{\Gamma} \\ \boldsymbol{O} & \boldsymbol{Q}^T\boldsymbol{\Gamma} & \boldsymbol{O} & \boldsymbol{O} & \boldsymbol{Q}^T\boldsymbol{\Gamma}_{,1} \\ \boldsymbol{O} & \boldsymbol{O} & \boldsymbol{Q}^T & \boldsymbol{O} & \boldsymbol{Q}^T\boldsymbol{Z}_{,2}\boldsymbol{\Gamma} \\ \boldsymbol{O} & \boldsymbol{O} & \boldsymbol{O} & \boldsymbol{Q}^T\boldsymbol{\Gamma} & \boldsymbol{Q}^T\boldsymbol{\Gamma}_{,2} \end{bmatrix}, \quad \boldsymbol{\Delta} = \begin{bmatrix} \boldsymbol{I}\frac{\partial}{\partial\xi_1} & \boldsymbol{O} \\ \boldsymbol{O} & \boldsymbol{I}\frac{\partial}{\partial\xi_1} \\ \boldsymbol{I}\frac{\partial}{\partial\xi_2} & \boldsymbol{O} \\ \boldsymbol{O} & \boldsymbol{I}\frac{\partial}{\partial\xi_2} \\ \boldsymbol{O} & \boldsymbol{I} \end{bmatrix} \text{ and } \dot{\boldsymbol{d}} = \begin{bmatrix} \dot{\boldsymbol{u}} \\ \dot{\boldsymbol{\theta}} \end{bmatrix}. \tag{53}$$

4 Statics

4.1 Generalized stresses

The jacobian of the displacement field mapping is given by

$$J = \det \boldsymbol{F} = \det\left(\boldsymbol{F}^{\mathrm{e}}\boldsymbol{F}^{\mathrm{o}}\right) = \det \boldsymbol{F}^{\mathrm{e}} \det \boldsymbol{F}^{\mathrm{o}} = J^{\mathrm{e}}J^{\mathrm{o}}, \tag{54}$$

where the effective jacobian is $J^{\mathrm{e}} = \det \boldsymbol{F}^{\mathrm{e}}$.

The effective first Piola-Kirchhoff stress tensor is given by

$$\boldsymbol{P}^{\mathrm{e}} = J^{\mathrm{e}}\boldsymbol{T}\boldsymbol{F}^{\mathrm{e}-T}, \tag{55}$$

where $\boldsymbol{T}$ is the Cauchy stress tensor. Solving for $\boldsymbol{T}$ in the previous equation and using (54), the total first Piola-Kirchhoff stress tensor yields

$$\boldsymbol{P} = J\boldsymbol{T}\boldsymbol{F}^{-T} = J\left(J^{\mathrm{e}-1}\boldsymbol{P}^{\mathrm{e}}\boldsymbol{F}^{\mathrm{e}T}\right)\boldsymbol{F}^{-T} = J^{\mathrm{o}}\boldsymbol{P}^{\mathrm{e}}\boldsymbol{F}^{\mathrm{o}-T}. \tag{56}$$

Taking into account (43) the latter equation can assume the form

$$\boldsymbol{P} = J^{\mathrm{o}}\boldsymbol{P}^{\mathrm{e}}\left(\frac{1}{J^{\mathrm{o}}}\left(\boldsymbol{e}_i^r \otimes \boldsymbol{g}_i^{\mathrm{o}r}\right)\boldsymbol{Q}^{\mathrm{o}T}\right)^T = \boldsymbol{P}^{\mathrm{e}}\boldsymbol{Q}^{\mathrm{o}}\left(\boldsymbol{g}_i^{\mathrm{o}r} \otimes \boldsymbol{e}_i^r\right). \tag{57}$$

As the effective first Piola-Kirchhoff stress tensor, $\boldsymbol{P}^{\mathrm{e}}$, can always be expressed by

$$\boldsymbol{P}^{\mathrm{e}} = \boldsymbol{\tau}_i^{\mathrm{e}} \otimes \boldsymbol{e}_i^{\mathrm{o}} = \boldsymbol{Q}\boldsymbol{\tau}_i^{\mathrm{e}r} \otimes \boldsymbol{e}_i^{\mathrm{o}} \tag{58}$$

equation (57) may be rewritten as

$$\boldsymbol{P} = \left(\boldsymbol{Q}\boldsymbol{\tau}_i^{\mathrm{e}r} \otimes \boldsymbol{e}_i^{\mathrm{o}}\right)\boldsymbol{Q}^{\mathrm{o}}\left(\boldsymbol{g}_j^{\mathrm{o}r} \otimes \boldsymbol{e}_j^r\right) = \boldsymbol{Q}\boldsymbol{\tau}_i^r \otimes \boldsymbol{e}_i^r, \tag{59}$$

where $\boldsymbol{\tau}_i^r = \left(\boldsymbol{g}_j^{\mathrm{o}r} \cdot \boldsymbol{e}_i^r\right)\boldsymbol{\tau}_i^{\mathrm{e}r}$ or

$$\boldsymbol{\tau}_\alpha^r = \left(\boldsymbol{g}_\alpha^{\mathrm{o}r} \cdot \boldsymbol{e}_\beta^r\right)\boldsymbol{\tau}_\beta^{\mathrm{e}r}, \tag{60a}$$

$$\boldsymbol{\tau}_3^r = \left(\boldsymbol{g}_\alpha^{\mathrm{o}r} \cdot \boldsymbol{e}_3^r\right)\boldsymbol{\tau}_3^{\mathrm{e}r} = \left(\boldsymbol{f}_1^{\mathrm{o}r} \cdot \boldsymbol{f}_2^{\mathrm{o}r} \times \boldsymbol{f}_3^{\mathrm{o}r}\right)\boldsymbol{\tau}_3^{\mathrm{e}r} = J^{\mathrm{o}}\boldsymbol{\tau}_3^{\mathrm{e}r}. \tag{60b}$$

As usual for linear models, the imposition of the plane stress assumption is made at the constitutive level. After the imposition of this plane stress state, the stress vectors are denoted by "$\widetilde{()}$". Accordingly, equations (58) and (59) are modified to

$$\boldsymbol{P}^{\mathrm{e}} = \boldsymbol{Q}\widetilde{\boldsymbol{\tau}}_i^{\mathrm{e}r} \otimes \boldsymbol{e}_i^{\mathrm{o}} \tag{61a}$$

$$\boldsymbol{P} = \boldsymbol{Q}\widetilde{\boldsymbol{\tau}}_i^{r} \otimes \boldsymbol{e}_i^{r} \tag{61b}$$

respectively and

$$\widetilde{\boldsymbol{\tau}}_\alpha^r = \left(\boldsymbol{g}_\alpha^{\mathrm{o}r} \cdot \boldsymbol{e}_\beta^r\right) \widetilde{\boldsymbol{\tau}}_\beta^{\mathrm{e}r}, \tag{62a}$$

$$\widetilde{\boldsymbol{\tau}}_3^r = J^{\mathrm{o}} \widetilde{\boldsymbol{\tau}}_3^{\mathrm{e}r}. \tag{62b}$$

4.2 Internal power

Resorting (56) and (42) and bearing in mind that $\dot{\boldsymbol{F}}^{\mathrm{o}} = \boldsymbol{O}$, the internal power per unit initial configuration volume is

$$\boldsymbol{P}^{\mathrm{e}} : \dot{\boldsymbol{F}}^{\mathrm{e}} = J^{\mathrm{o}-1} \boldsymbol{P}\boldsymbol{F}^{\mathrm{o}T} : \dot{\boldsymbol{F}}\boldsymbol{F}^{\mathrm{o}-1} = J^{\mathrm{o}-1} \boldsymbol{P} : \dot{\boldsymbol{F}}. \tag{63}$$

It is possible to write the internal power per unit reference configuration volume as

$$\boldsymbol{P} : \dot{\boldsymbol{F}} = \widetilde{\boldsymbol{\tau}}_\alpha^r \cdot \dot{\boldsymbol{\gamma}}_\alpha^r = \widetilde{\boldsymbol{\tau}}_\alpha^r \cdot \dot{\boldsymbol{\eta}}_\alpha^r + \boldsymbol{a}^r \times \widetilde{\boldsymbol{\tau}}_\alpha^r \cdot \dot{\boldsymbol{\kappa}}_\alpha^r, \tag{64}$$

where the symmetry condition $\boldsymbol{P}\boldsymbol{F}^T = \left(\boldsymbol{P}\boldsymbol{F}^T\right)^T$ was introduced.

Noticing that $\mathrm{d}V^{\mathrm{o}} = J^{\mathrm{o}}\mathrm{d}V^r$ and using the former equation, the total internal power follows as

$$P_{\mathrm{int}} = \int_{V^{\mathrm{o}}} \boldsymbol{P}^{\mathrm{e}} : \dot{\boldsymbol{F}}^{\mathrm{e}} \mathrm{d}V^{\mathrm{o}} = \int_{\Omega^r} \left(\boldsymbol{n}_\alpha^r \cdot \dot{\boldsymbol{\eta}}_\alpha^r + \boldsymbol{m}_\alpha^r \cdot \dot{\boldsymbol{\kappa}}_\alpha^r\right) \mathrm{d}\Omega^r, \tag{65}$$

where the following stress resultants where introduced

$$\boldsymbol{n}_\alpha^r = \int_{H^r} \widetilde{\boldsymbol{\tau}}_\alpha^r \mathrm{d}H^r, \qquad \boldsymbol{m}_\alpha^r = \int_{H^r} \boldsymbol{a}^r \times \widetilde{\boldsymbol{\tau}}_\alpha^r \mathrm{d}H^r. \tag{66}$$

Collecting this generalized forces in the $\boldsymbol{\sigma}^r$ vector as

$$\boldsymbol{\sigma}^r = \begin{bmatrix} \boldsymbol{\sigma}_1^r \\ \boldsymbol{\sigma}_2^r \end{bmatrix} \text{ and } \boldsymbol{\sigma}_\alpha^r = \begin{bmatrix} \boldsymbol{n}_\alpha^r \\ \boldsymbol{m}_\alpha^r \end{bmatrix} \tag{67}$$

the internal power can assume the compact form

$$P_{\mathrm{int}} = \int_{\Omega^r} \boldsymbol{\sigma}^r \cdot \dot{\boldsymbol{\varepsilon}}^r \mathrm{d}\Omega^r. \tag{68}$$

4.3 External power

The external power may be expressed as[6]

$$\begin{aligned} P_{\text{ext}} = &\int_{\Omega^{\text{o}t}} \overline{\boldsymbol{t}}^{\text{o}t} \cdot \dot{\boldsymbol{x}} \mathrm{d}\Omega^{\text{o}t} + \int_{\Omega^{\text{o}b}} \overline{\boldsymbol{t}}^{\text{o}b} \cdot \dot{\boldsymbol{x}} \mathrm{d}\Omega^{\text{o}b} + \int_{V^{\text{o}}} \overline{\boldsymbol{b}}^{\text{o}} \cdot \dot{\boldsymbol{x}} \mathrm{d}V^{\text{o}} \\ &+ \int_{\Gamma_t^{\text{o}}} \int_{H^{\text{o}}} \overline{\boldsymbol{t}}^{\text{o}l} \cdot \dot{\boldsymbol{x}} \mathrm{d}H^{\text{o}} \mathrm{d}\Gamma_t^{\text{o}} + \int_{\Gamma_u^{\text{o}}} \int_{H^{\text{o}}} \boldsymbol{r}^{\text{o}} \cdot \dot{\boldsymbol{x}} \mathrm{d}H^{\text{o}} \mathrm{d}\Gamma_u^{\text{o}} \end{aligned} \tag{69}$$

where $\boldsymbol{r}^{\text{o}}$ are the reaction tractions on the kinematic boundary, per unit area of the initial configuration. The former equation can easily be rewritten in the reference configuration as

$$\begin{aligned} P_{\text{ext}} = &\int_{\Omega^r} \left(\overline{\boldsymbol{t}}^t \cdot \dot{\boldsymbol{x}} + \overline{\boldsymbol{t}}^b \cdot \dot{\boldsymbol{x}} + \int_{H^r} \overline{\boldsymbol{b}} \cdot \dot{\boldsymbol{x}} \mathrm{d}H^r \right) \mathrm{d}\Omega^r \\ &+ \int_{\Gamma_t^r} \int_{H^r} \overline{\boldsymbol{t}}^l \cdot \dot{\boldsymbol{x}} \mathrm{d}H^r \mathrm{d}\Gamma_t^r + \int_{\Gamma_u^r} \int_{H^r} \boldsymbol{r} \cdot \dot{\boldsymbol{x}} \mathrm{d}H^r \mathrm{d}\Gamma_u^r, \end{aligned} \tag{70}$$

if we introduce the definitions[7] $\overline{\boldsymbol{t}}^{\text{o}t} = J^{\text{o}t}\overline{\boldsymbol{t}}^t$, $\overline{\boldsymbol{t}}^{\text{o}b} = J^{\text{o}b}\overline{\boldsymbol{t}}^b$, $\overline{\boldsymbol{t}}^{\text{o}l} = J^{\text{o}l}\overline{\boldsymbol{t}}^l$ and $\overline{\boldsymbol{r}}^{\text{o}} = J^{\text{o}l}\overline{\boldsymbol{r}}$ with the notation for the transformation jacobians $\mathrm{d}V^{\text{o}} = J^{\text{o}}\mathrm{d}V^r$, $\mathrm{d}\Omega^{\text{o}t} = J^{\text{o}t}\mathrm{d}\Omega^r$, $\mathrm{d}\Omega^{\text{o}b} = J^{\text{o}b}\mathrm{d}\Omega^r$, $\mathrm{d}\Gamma_t^{\text{o}} = J^{\text{o}l}\mathrm{d}\Gamma_t^r$ and $\mathrm{d}\Gamma_u^{\text{o}} = J^{\text{o}l}\mathrm{d}\Gamma_u^r$.

Introducing (20) in (19) and performing time differentiation on both sides and then substituting the result in (70) yields

$$\begin{aligned} P_{\text{ext}} = &\int_{\Omega^r} \left(\overline{\boldsymbol{n}}^{\Omega} \cdot \dot{\boldsymbol{u}} + \overline{\boldsymbol{m}}^{\Omega} \cdot \boldsymbol{\omega} \right) \mathrm{d}\Omega^r + \int_{\Gamma_t^r} \left(\overline{\boldsymbol{n}}^{\Gamma} \cdot \dot{\boldsymbol{u}} + \overline{\boldsymbol{m}}^{\Gamma} \cdot \boldsymbol{\omega} \right) \mathrm{d}\Gamma_t^r \\ &+ \int_{\Gamma_u^r} \left(\boldsymbol{n}^{\Gamma} \cdot \dot{\boldsymbol{u}} + \boldsymbol{m}^{\Gamma} \cdot \boldsymbol{\omega} \right) \mathrm{d}\Gamma_u^r, \end{aligned} \tag{71}$$

where

$$\overline{\boldsymbol{n}}^{\Omega} = \overline{\boldsymbol{t}}^t + \overline{\boldsymbol{t}}^b + \int_{H^r} \overline{\boldsymbol{b}} \mathrm{d}H^r, \tag{72a}$$

$$\overline{\boldsymbol{n}}^{\Gamma} = \int_{H^r} \overline{\boldsymbol{t}}^l \mathrm{d}H^r, \tag{72b}$$

$$\boldsymbol{n}^{\Gamma} = \int_{H^r} \boldsymbol{r} \mathrm{d}H^r, \tag{72c}$$

[6] The superscripts l, t and b stand for *lateral*, *top* and *bottom*, respectively.
[7] The superscript l stands for *lateral*.

and

$$\overline{\boldsymbol{m}}^{\Omega} = \boldsymbol{a}^t \times \overline{\boldsymbol{t}}^t + \boldsymbol{a}^b \times \overline{\boldsymbol{t}}^b + \int_{H^r} \boldsymbol{a} \times \overline{\boldsymbol{b}} \mathrm{d}H^r, \tag{73a}$$

$$\overline{\boldsymbol{m}}^{\Gamma} = \int_{H^r} \boldsymbol{a} \times \overline{\boldsymbol{t}}^l \mathrm{d}H^r, \tag{73b}$$

$$\boldsymbol{m}^{\Gamma} = \int_{H^r} \boldsymbol{a} \times \boldsymbol{r} \mathrm{d}H^r. \tag{73c}$$

are cross-sectional generalized resultants per unit length of the reference configuration and the superscripts Ω^r and Γ_t^r were simplified to Ω and Γ, as no danger of misinterpretation exists.

It is possible to achieve a even more compact form for the external power. By defining the vectors

$$\overline{\boldsymbol{q}}^{\Omega} = \begin{bmatrix} \overline{\boldsymbol{n}}^{\Omega} \\ \overline{\boldsymbol{\mu}}^{\Omega} \end{bmatrix} \qquad \overline{\boldsymbol{q}}^{\Gamma} = \begin{bmatrix} \overline{\boldsymbol{n}}^{\Gamma} \\ \overline{\boldsymbol{\mu}}^{\Gamma} \end{bmatrix} \qquad \boldsymbol{q}^{\Gamma} = \begin{bmatrix} \boldsymbol{n}^{\Gamma} \\ \boldsymbol{\mu}^{\Gamma} \end{bmatrix} \tag{74}$$

the expression of the external power (71) reads

$$P_{\text{ext}} = \int_{\Omega^r} \overline{\boldsymbol{q}}^{\Omega} \cdot \dot{\boldsymbol{d}} \mathrm{d}\Omega^r + \int_{\Gamma_t^r} \overline{\boldsymbol{q}}^{\Gamma} \cdot \dot{\boldsymbol{d}} \mathrm{d}\Gamma_t^r + \int_{\Gamma_u^r} \boldsymbol{q}^{\Gamma} \cdot \dot{\boldsymbol{d}} \mathrm{d}\Gamma_u^r. \tag{75}$$

Here, $\overline{\boldsymbol{q}}^{\Omega}$ is the vector resulting from the external loading along the shell middle plane per reference are unit, $\overline{\boldsymbol{q}}^{\Gamma}$ is the vector resulting from the external loading on the static boundary and $\boldsymbol{q}^{\Gamma}$ is the vector resulting from the tractions on the kinematic boundary. Notice that $\overline{\boldsymbol{\mu}}^{\Omega} = \boldsymbol{\Gamma}^T \overline{\boldsymbol{m}}^{\Omega}$, $\overline{\boldsymbol{\mu}}^{\Gamma} = \boldsymbol{\Gamma}^T \overline{\boldsymbol{m}}^{\Gamma}$ and $\boldsymbol{\mu}^{\Gamma} = \boldsymbol{\Gamma}^T \boldsymbol{m}^{\Gamma}$ are pseudo-moments which are energetically conjugated with $\dot{\boldsymbol{\theta}}$. Notice that the true power conjugate of $\dot{\boldsymbol{\theta}}$ is not simply the moment resultants as usually happens on geometrically linear theories.

5 Variational formulation of the problem

5.1 A constrained weak form

It is possible to show that the variation of the generalized strain vector is

$$\delta\boldsymbol{\gamma}_{\alpha}^r = \delta\boldsymbol{\eta}_{\alpha}^r + \delta\boldsymbol{\kappa}_{\alpha}^r \times \boldsymbol{a}^r \tag{76}$$

and

$$\delta\boldsymbol{\eta}_{\alpha}^r = \boldsymbol{Q}^T \left(\delta\boldsymbol{u}_{,\alpha} + \boldsymbol{Z}_{,\alpha} \boldsymbol{\Gamma} \delta\boldsymbol{\theta} \right), \tag{77a}$$

$$\delta\boldsymbol{\kappa}_{\alpha}^r = \boldsymbol{Q}^T \left(\boldsymbol{\Gamma}_{,\alpha} \delta\boldsymbol{\theta} + \boldsymbol{\Gamma} \delta\boldsymbol{\theta}_{,\alpha} \right). \tag{77b}$$

Resorting to (52)

$$\delta\boldsymbol{\varepsilon}^r = \boldsymbol{\Psi} \boldsymbol{\Delta} \delta\boldsymbol{d}. \tag{78}$$

In view of (65) the internal virtual work may, thus, be written as

$$\delta W_{\text{int}} = \int_{\Omega^r} \boldsymbol{\sigma}^r \cdot \delta \boldsymbol{\varepsilon}^r \mathrm{d}\Omega^r. \tag{79}$$

The external virtual work is

$$\delta W_{\text{ext}} = \int_{\Omega^r} \overline{\boldsymbol{q}}^{\Omega} \cdot \delta \boldsymbol{d} \mathrm{d}\Omega^r + \int_{\Gamma_t^r} \overline{\boldsymbol{q}}^{\Gamma} \cdot \delta \boldsymbol{d} \mathrm{d}\Gamma_t^r + \int_{\Gamma_u^r} \boldsymbol{q}^{\Gamma} \cdot \delta \boldsymbol{d} \mathrm{d}\Gamma_u^r. \tag{80}$$

Notice the inclusion of the Virtual Work arising from the kinematic boundary, given by the projection of the generalized reactions on the virtual displacements.

The weak form of the equilibrium of the rod can be recast by the following virtual work principle

$$\delta W_{\text{int}} - \delta W_{\text{ext}} = 0, \quad \forall\, \delta \boldsymbol{d} \tag{81}$$

where $\delta \boldsymbol{d}$ stands for an infinitesimal perturbation of the generalized displacements field.

Let us now assume that the prescribed displacements are given as

$$\overline{\boldsymbol{d}} = \begin{bmatrix} \overline{\boldsymbol{u}} \\ \overline{\boldsymbol{\theta}} \end{bmatrix}, \tag{82}$$

i. e., we assume that the prescribed orientation of the kinematic part of the contour of the shell is already in terms of the Euler-Rodrigues parameters. In general, a rotation tensor can be used to prescribe the displacements. In this case an extraction procedure should be applied, see [14].

The weak imposition of the kinematic boundary conditions reads[8]

$$-\int_{\Gamma_u^r} \delta \boldsymbol{q}^{\Gamma} \cdot \left(\boldsymbol{d} - \overline{\boldsymbol{d}}\right) \mathrm{d}\Gamma_u^r = 0, \quad \forall\, \delta \boldsymbol{q}^{\Gamma}. \tag{83}$$

The combination of the Principle of Virtual Work (81) and the weak constraint imposition (83) gives the final weak form, which is the following hybrid functional

$$\delta W = 0, \tag{84}$$

where

$$\begin{aligned} \delta W = &\int_{\Omega^r} \boldsymbol{\sigma}^r \cdot \delta \boldsymbol{\varepsilon}^r \mathrm{d}\Omega^r - \int_{\Omega^r} \overline{\boldsymbol{q}}^{\Omega} \cdot \delta \boldsymbol{d} \mathrm{d}\Omega^r - \int_{\Gamma_t^r} \overline{\boldsymbol{q}}^{\Gamma} \cdot \delta \boldsymbol{d} \mathrm{d}\Gamma_t^r \\ &- \int_{\Gamma_u^r} \boldsymbol{q}^{\Gamma} \cdot \delta \boldsymbol{d} \mathrm{d}\Gamma_u^r - \int_{\Gamma_u^r} \delta \boldsymbol{q}^{\Gamma} \cdot \left(\boldsymbol{d} - \overline{\boldsymbol{d}}\right) \mathrm{d}\Gamma_u^r. \end{aligned} \tag{85}$$

Combinations of variational statements were extensively used for generating generalized principles for linear analysis. Here the extension for nonlinear analysis is accomplished.

[8]The convenience of the introduction of the minus sign is associated with (i) the attainment of a symmetric linearized weak form and (ii) the possibility of identifying $\boldsymbol{q}^{\Gamma}$ with the generalized reaction force.

If the problem under analysis is conservative, the variational form could be derived from a constrained stationary potential energy principle.

Besides the usual requirements in order the integrals in (85) make sense, no additional restrictions are demanded. In particular, the usual $\delta \boldsymbol{d} = \boldsymbol{o}$ on the kinematic boundary points, Γ_u^r, is avoided in order to be able to use approximations not fulfilling the Kronecker-delta property.

6 A meshfree method

6.1 The approximation functions

The approximation of the *six* generalized displacements fields over the *plane* reference system is made through MLS nodal functions. The use of this complex and computationally demanding, relatively to the polynomial nodal shape functions used by common FEM, functions is justified by their (i) reproducing properties and (ii) inherent prescribed continuity (which is limited by the basis and/or the bell-shaped weight function).

For the static boundary, simple Lagrange polynomials can be used, but other options are also possible, like one-dimensional MLS, see [15].

Hence, consider the following approximations

$$\boldsymbol{d} = \boldsymbol{\Phi}^{\Omega}\mathbf{d} \qquad \boldsymbol{q}^{\Gamma} = \boldsymbol{\Phi}^{\Gamma}\mathbf{q}^{\Gamma} \tag{86a}$$

$$\delta\boldsymbol{d} = \boldsymbol{\Phi}^{\Omega}\delta\mathbf{d} \qquad \delta\boldsymbol{q}^{\Gamma} = \boldsymbol{\Phi}^{\Gamma}\delta\mathbf{q}^{\Gamma} \tag{86b}$$

$$\Delta\boldsymbol{d} = \boldsymbol{\Phi}^{\Omega}\Delta\mathbf{d} \qquad \Delta\boldsymbol{q}^{\Gamma} = \boldsymbol{\Phi}^{\Gamma}\Delta\mathbf{q}^{\Gamma} \tag{86c}$$

where, a possibility is to choose,

$$\boldsymbol{\Phi}^{\Omega} = \begin{bmatrix} \phi_1^{\Omega}\mathbf{I} & \mathbf{O} & \cdots & \phi_n^{\Omega}\mathbf{I} & \mathbf{O} \\ \mathbf{O} & \phi_1^{\Omega}\mathbf{I} & & \mathbf{O} & \phi_n^{\Omega}\mathbf{I} \end{bmatrix} \qquad \boldsymbol{\Psi} = \begin{bmatrix} \phi_1^{\Gamma}\mathbf{I} & \mathbf{O} & \cdots & \phi_n^{\Gamma}\mathbf{I} & \mathbf{O} \\ \mathbf{O} & \phi_1^{\Gamma}\mathbf{I} & & \mathbf{O} & \phi_n^{\Gamma}\mathbf{I} \end{bmatrix}. \tag{87}$$

Here the functions ϕ^{Ω} are MLS functions and ϕ^{Γ} are linear Lagrange polynomials.

Frequently the measures of the error of the FEM are based on the discontinuities of the stress fields (i) between elements and (ii) on the static boundary. In the present formulation possible measures of the error can be derived from (i) on the discontinuity of the generalized stresses on the static boundary, (ii) on the error between the independently approximated generalized stresses on the kinematic boundary and the same stresses evaluated from the domain approximation and (iii) on the error in the imposed displacements.

6.2 Discretized form of the residual vector and generalized tangent stiffness matrix

The use of the approximations (86) in the hybrid functional (85), after some algebraic manipulations, yields

$$\mathbf{R} = \mathbf{0} \qquad \forall \delta\mathbf{d}, \delta\mathbf{q}^{\Gamma}, \tag{88}$$

where $\mathbf{R}$ is the the residual vector

$$\mathbf{R} = \begin{bmatrix} \mathbf{P} + \mathbf{B}\mathbf{q}^{\Gamma} \\ \mathbf{B}^T\mathbf{d} + \mathbf{v} \end{bmatrix} \tag{89}$$

and

$$\mathbf{P} = \int_{\Omega^r} \left(\boldsymbol{\Delta}\boldsymbol{\Phi}^{\Omega}\right)^T \boldsymbol{\Psi}^T \boldsymbol{\sigma}^r \mathrm{d}\Omega^r - \int_{\Omega^r} \boldsymbol{\Phi}^{\Omega T}\overline{\boldsymbol{q}}^{\Omega}\mathrm{d}\Omega^r - \int_{\Gamma_t^r} \boldsymbol{\Phi}^{\Omega T}\overline{\boldsymbol{q}}^{\Gamma}\mathrm{d}\Gamma_t^r, \tag{90a}$$

$$\mathbf{B} = -\int_{\Gamma_u^r} \boldsymbol{\Phi}^{\Gamma T}\boldsymbol{\Psi}\mathrm{d}\Gamma_u^r, \tag{90b}$$

$$\mathbf{v} = \int_{\Gamma_u^r} \boldsymbol{\Phi}^{\Gamma T}\overline{\boldsymbol{d}}\mathrm{d}\Gamma_u^r. \tag{90c}$$

The use of the approximations (86) in the generalized tangent form yields, after some algebraic manipulations,

$$\mathbf{K}\Delta\mathbf{a} \qquad \forall\delta\mathbf{d}, \delta\mathbf{q}^{\Gamma}, \tag{91}$$

where

$$\mathbf{K} = \begin{bmatrix} \mathbf{S} & \mathbf{B} \\ \mathbf{B}^T & \mathbf{0} \end{bmatrix} \qquad \text{and} \qquad \Delta\mathbf{a} = \begin{bmatrix} \Delta\mathbf{d} \\ \Delta\mathbf{q}^{\Gamma} \end{bmatrix} \tag{92}$$

and $\mathbf{S}$ is the the generalized stiffness matrix

$$\begin{aligned} \mathbf{S} = &\int_{\Omega^r} \left(\left(\boldsymbol{\Delta}\boldsymbol{\Phi}^{\Omega}\right)^T \boldsymbol{\Psi}^T \boldsymbol{D}\, \boldsymbol{\Psi} \left(\boldsymbol{\Delta}\boldsymbol{\Phi}^{\Omega}\right) + \left(\boldsymbol{\Delta}\boldsymbol{\Phi}^{\Omega}\right)^T \boldsymbol{G} \left(\boldsymbol{\Delta}\boldsymbol{\Phi}^{\Omega}\right) - \boldsymbol{\Phi}^{\Omega T}\boldsymbol{L}^{\Omega}\boldsymbol{\Phi}^{\Omega} \right) \mathrm{d}\Omega^r \\ &- \int_{\Gamma_t^r} \boldsymbol{\Phi}^{\Gamma T}\boldsymbol{L}^{\Gamma}\boldsymbol{\Phi}^{\Gamma}\mathrm{d}\Gamma_t^r, \end{aligned} \tag{93}$$

where $\boldsymbol{D}$, $\boldsymbol{G}$, $\boldsymbol{L}^{\Omega}$ and $\boldsymbol{L}^{\Gamma}$ are the constitutive, geometric, load on the domain and load on the static boundary generalized tangent stiffness operators. The definition of these can be found on [7], except for the last term, which was not taken into account in those works. Nevertheless, its value can be inferred from $\boldsymbol{L}^{\Omega}$. For conservative loadings, these two latter matrix operators are always symmetric. For the common case of only applied load on the middle surface both of these operators are null.

The identification of the location of the bifurcation points is made by the study of the eigenvalues of the discretized form of the generalized tangent stiffness matrix $(92)_1$. If consistent approximations are used, in order to eliminate the *shear locking* effects, then the dependencies introduced via the approximation should be taken into account, because they give rise to (numerically) null eigenvalues. Also, for each kinematic boundary variable a negative eigenvalue will appear. The rule for determining the exact number of null eigenvalues is given in [16].

In the frequent case were the shell middle surface is not smooth and is, in fact, an assembly of several smooth shells, it is also possible to analyze the all set by including continuity conditions on the intersections in the weak form (85). Of course, extra degrees of freedom will be associated to the intersection and the residual vector (89) and the generalized tangent form (92) will exhibit a somewhat complex form.

7 Implementation aspects

7.1 Evaluation of the nodal approximation functions

The success of the presented method crucially depends on (i) the accuracy and (ii) the performance of the evaluation of the nodal functions.

The accuracy of the evaluation of the nodal functions is intimately linked to the discretization adopted and the size of the reference domain, because the moments matrix present in the normal system of equations, to be solved during the MLS functions evaluation, can be poorly conditioned. A very efficient way of solving this problem is the use of a local coordinate system *centered* at the sample (usually Gauss) point. In this way the performance is not affected and the moment matrix is always well conditioned[9].

As for the performance of the evaluation of the nodal functions, two aspects should be taken into account. On one hand, the inversion of the moments matrix and their derivatives should be avoided, as described in [17]. On the other hand, as the values of the nodal functions and their derivatives, at the integration points, are required many times along the incremental/iterative process, it is desirable to evaluate and store them at the beginning of the process.

7.2 A generalized arc-length method

The solution of the resulting nonlinear system of equations (88) is achieved by the use of an incremental/iterative approach. The full Newton-Raphson method should be combined with some (non-physical) constraint in order to trace the full loading path of the shell.

To be consistent with the approximations made, this constraint should not include only generalized displacements and loads, but also should render the generalized boundary tractions on the kinematic boundary. Therefore, the following arc-length constraint that nonlinearly relates the incremental/iterative generalized displacements, forces and load parameter with a certain constant, the arc-length Δl, is introduced

$$\Delta\mathbf{d}^T\mathbf{W}^{\boldsymbol{d}}\Delta\mathbf{d} + \Delta\theta^T\mathbf{W}^{\boldsymbol{\theta}}\Delta\theta + \Delta\mathbf{n}^{\lambda T}\mathbf{W}^{\boldsymbol{n}}\Delta\mathbf{n}^{\lambda} + \Delta\mathbf{m}^{\lambda T}\mathbf{W}^{\boldsymbol{m}}\Delta\mathbf{m}^{\lambda} + \psi 2\Delta\lambda 2 = \Delta l 2, \tag{94}$$

where $\mathbf{W}$'s are weighting matrices which are, at least, positive semi-definite diagonals and ψ is also a scaling parameter. Thus, the method presented by [18] was generalized in order to include the essential boundary reactions, resulting in a robust and fast procedure.

7.3 The initial configuration description

The initial configuration can be expressed by several ways. An obvious procedure, used for linear shell analysis in [19], is to resource MLS. In this way a sort of *isoparametric* approximation is performed. Nevertheless, there is no reason why the *exact* initial configuration should not be used. In this way the title of this work is justified in the present context.

[9] Of course, the usual conditions on the number of points in the support and their disposition also apply here.

The mapping to the initial configuration defined by (3) is now materialized. In the present work only four mapping types were used. This were sufficient to analyze most of the benchmark test proposed in the literature.

7.4 Polynomial

A polynomial mapping is defined as

$$\boldsymbol{z}^{\mathrm{o}}\left(\xi_1,\xi_2\right)=\sum_{i=0}^{p}\sum_{j=0}^{q}\boldsymbol{a}_{ij}\xi_1^i\xi_2^j, \tag{95}$$

where $\boldsymbol{a}_{ij}$ are vectors collecting the coefficients of the polynomial mapping including all terms of degree p and q in the $\boldsymbol{e}_1^r$ and $\boldsymbol{e}_2^r$ directions, respectively.

7.5 Cylindrical

A cylindrical mapping is defined as

$$\boldsymbol{z}^{\mathrm{o}}\left(\xi_1,\xi_2\right)=\boldsymbol{\delta}^{\mathrm{o}}+\begin{bmatrix}\xi_1\\ r\cos\left(\frac{\xi_2}{r}\right)\\ r\sin\left(\frac{\xi_2}{r}\right)\end{bmatrix}, \tag{96}$$

where r is the radius of the cylinder and $\boldsymbol{\delta}^{\mathrm{o}}$ represents a rigid body translation.

7.6 Spherical

A spherical mapping is defined as

$$\boldsymbol{z}^{\mathrm{o}}\left(\xi_1,\xi_2\right)=\boldsymbol{\delta}^{\mathrm{o}}+\begin{bmatrix}r\sin\left(\frac{\xi_2}{r}\right)\cos\left(\frac{\xi_1}{r}\right)\\ r\sin\left(\frac{\xi_2}{r}\right)\sin\left(\frac{\xi_1}{r}\right)\\ r\cos\left(\frac{\xi_2}{r}\right)\end{bmatrix}, \tag{97}$$

where the meaning of the variables is the same relatively to the cylindrical mapping case.

The introduction of the radius r in the cylindrical and spherical angular coordinates is only a mean to obtain length dimensions in all coordinates. This is not mandatory, as discretization in angular dimensions does not introduce any special problem if the support is adequately chosen.

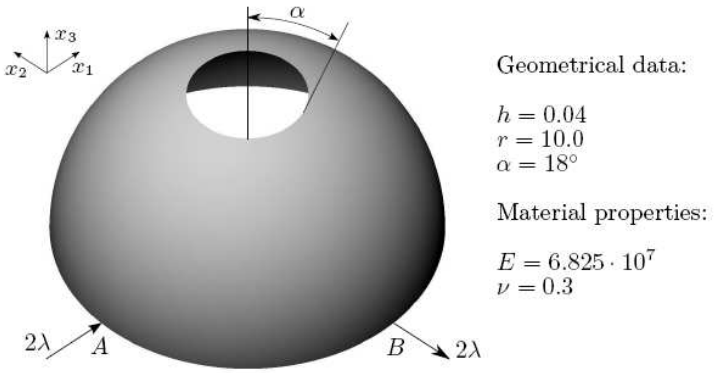

Figure 2: Data for pinched hemispherical.

8 Numerical example

Consider the double symmetric hemispherical shell of radius r with a 18° hole presented in figure (2) subjected to four concentrated loads[10]. In this Neumann problem the generalized boundary tractions, $\overline{\boldsymbol{q}}^{\Gamma}$, are null at all edges except in the four load application points.

This is one of the most spread benchmark tests for shell finite elements. Its linear analysis is included in the standard set of test problems proposed by [20].

Taking advantage of the double symmetry, only a quarter of the hemispherical shell is analyzed. The resulting problem still has a unrestraint rigid body motion along the x_3 direction. The imposition of punctual kinematic restraints is done exactly in the same way as its side counterpart. As the restrain refers to a point, the discretization degenerates in a scalar unknown. This methodology was used to prescribe the u_3 displacement at point A, see figure 2.

The initial configuration, Ω^{o}, was mapped from a reference configuration, Ω^{r}, resorting the spherical mapping, given by (97). In this case the reference configuration consists in rectangle with dimensions $[0, \frac{\pi}{2}r] \times [\frac{\pi}{10}r, \frac{\pi}{2}r]$.

Notice that the structure is still symmetric and is subjected to an antisymmetric loading. For linear analysis the convenient simplification would be advantageous. However, for the fully nonlinear testing, as intended in the present work, this simplification is not possible.

This particular problem presents an excellent tests to the membrane locking presence, as the shell practically bends without stretching, *i. e.* is nearly inextensional. As no specific device is being used to avoid membrane locking, it is expected pour accuracy of the results for low order basis. In fact, this was confirmed by numerical tests and only with a complete quintic basis the membrane locking was virtually removed from the solution.

For the trace of the response we use for the MLS approximation on the domain a complete quintic

[10] Two of loads are hidden behind the shell.

basis and an C^3 spline weight function. The use of this basis also prevents the shear locking occurrence and avoids the necessity of using the consistent approximation. The support dimension parameter was made equal to 1.5 on both $\boldsymbol{e}_\alpha^r$ directions.

We use this example to test the convergence of the solution with the increase of the number of points in the domain and kinematic boundary, constrained to be the same in both directions, $\boldsymbol{e}_\alpha^r$. Moreover, the number of points for the domain approximations and for the generalized boundary tractions was also equalized. We tested meshes of 11×11, 16×16 and 21×21 points, here denoted by discretizations I, II and III, respectively, and displayed in figure 3 on the reference configuration, Ω^r.

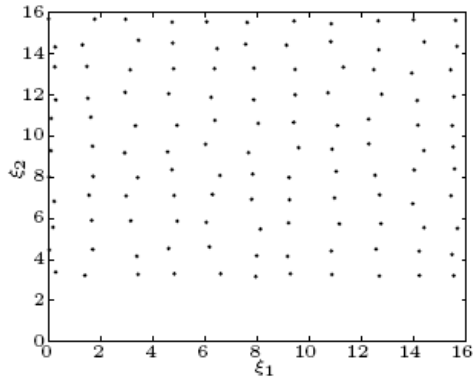

(a) Discretization I: 11×11 points.

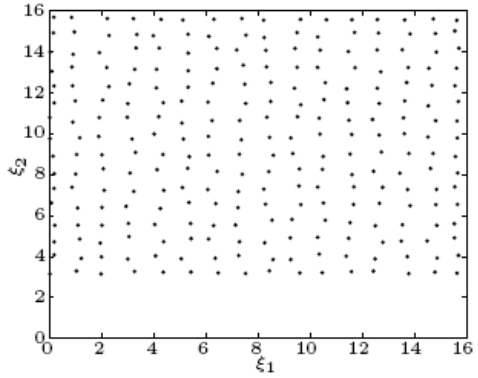

(b) Discretization II: 16×16 points.

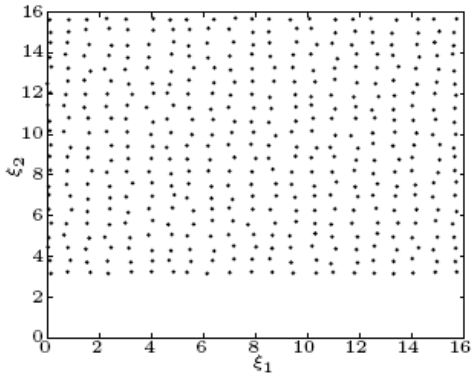

(c) Discretization III: 21×21 points.

Figure 3: The nodal discretizations used for the approximations on the reference configuration, Ω^r, of pinched hemispherical test.

In each of the analysis the domain integrations were carried out using a uniform cell structure of

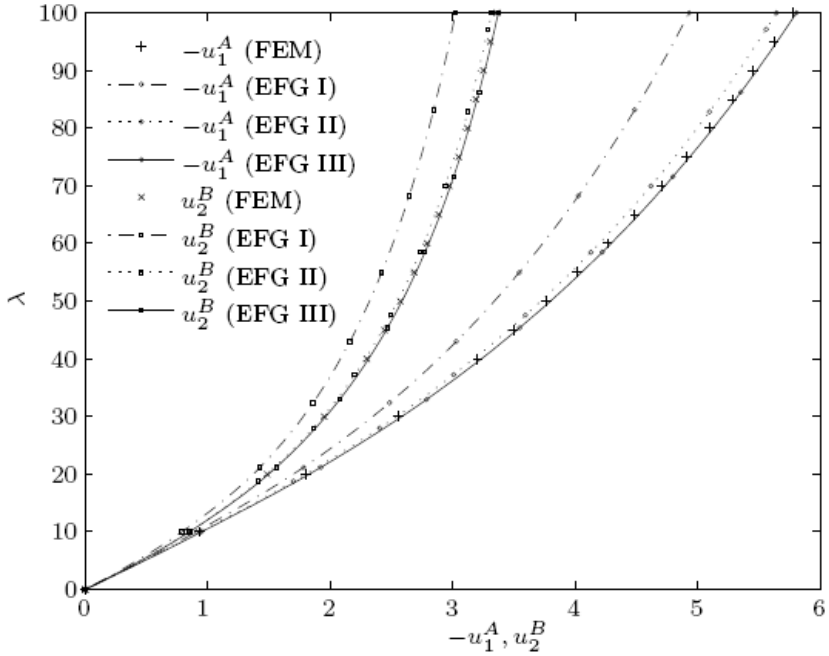

Figure 4: EFG response for pinched hemispherical at points A and B, see figure 2.

10×10, 15×15 and 20×20 integration cells for the discretizations I, II and III, respectively. Within each cell 3×3 sample points were used. The integration in the thickness direction was performed using 3 integration points.

The kinematical boundary integrations extend over the sides characterized by $\xi_1 = 0$ and $\xi_1 = \frac{\pi}{2} r$ of the reference configuration. These integrations were carried out using 10, 15 and 20 integration cells for the discretizations I, II and III, respectively. Within each of these cells, 5 sample points were employed.

The solution was generated using the Newton/Raphson method.

The obtained response for the displacements in points A and B along the normal direction to the shell, see figure 2, are presented in figure 4. The results are compared with a FEM solution of 32×32 elements with 65×65 nodes.

The slope at the origin of the trajectories $\lambda - (-u_1^A)$ and $\lambda - u_2^B$ represented in figure 4 converges exactly to same value. This fact is a direct consequence of the antisymmetry of the loading as, in the linear case, the displacements $-u_1^A$ and u_2^B under the loads are exactly the same.

The deformed shapes at selected steps are shown in figure 5 for discretization III.

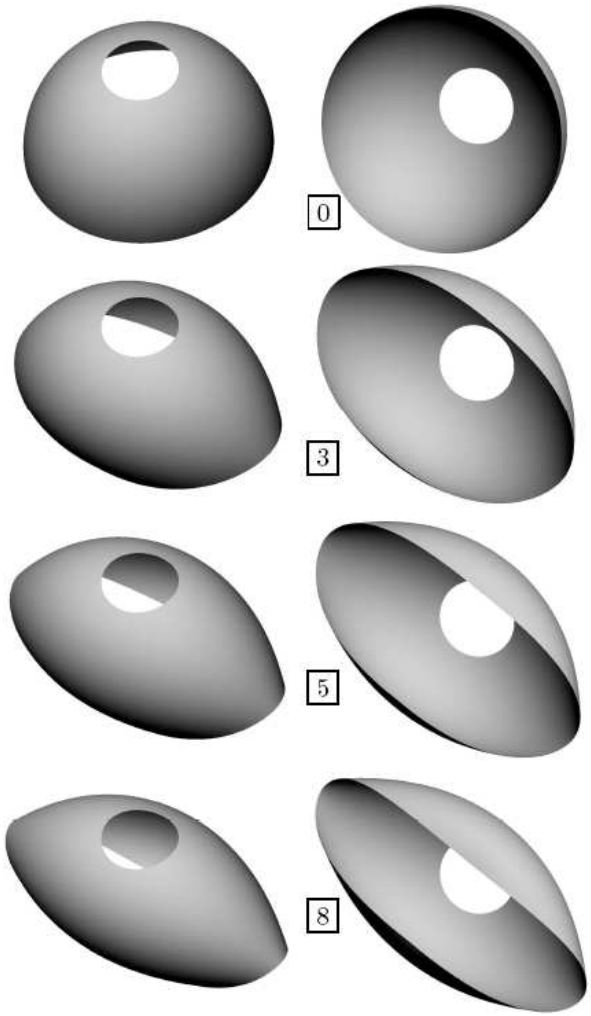

Figure 5: Deformed shapes for pinched hemispherical at selected steps for discretization III.

9 Conclusions

A meshless method for the structural analysis of shells was presented. The arbitrary initial geometry of the shell is exactly considered. A geometrically-exact approach was incorporated in a hybrid functional and the essential boundary conditions are imposed via Lagrange multipliers. The constitutive tensor is derived from a three dimensional material law by a plane stress imposition and allows the consideration

of finite strains. The solution space on the domain is projected on to the MLS nodal functions space. The resultant generalized stresses and displacements are continuous. Several implementation aspects were discussed and a numerical example is presented.

Acknowledgements

The first author would like to express his gratitude to Fundação Calouste Gulbenkian for supporting his staying in São Paulo, Brasil (grant 63179).

This work was carried out in the framework of the research activities of ICIST, Instituto de Engenharia de Estruturas, Território e Construção, and was funded by Fundação para a Ciência e Tecnologia, FEDER and the POCI program.

The second author would like to acknowledge the financial support by the CNPq, Conselho Nacional de Pesquisa of Brazil, and the DFG, Deutsche Forschungsgemeinschaft, during his stay at the IBNM of the Leibniz University of Hanover.

References

[1] Simo, J.C. & Fox, D.D., On a stress resultant geometrically exact shell model. Part I: formulation and optimal parametrization. *Computer Methods in Applied Mechanics and Engineering*, **72(3)**, pp. 267–304, 1989.

[2] Pimenta, P.M., On the geometrically–exact finite–strain rod model. *Proceeding of the third Pan–American Congress on Applied Mechanics, PACAM III*, Escola Politécnica da Universidade de São Paulo, Brazil, pp. 279–282, 1993.

[3] Pimenta, P.M., On the geometrically–exact finite–strain shell model. *Proceeding of the third Pan–American Congress on Applied Mechanics, PACAM III*, Escola Politécnica da Universidade de São Paulo, Brazil, pp. 616–619, 1993.

[4] Pimenta, P.M. & Yojo, T., Geometrically exact analysis of spatial frames. *Applied Mechanics Reviews*, **46(11)**, pp. 118–128, 1993.

[5] Pimenta, P.M., Geometrically exact analysis of initially curved rods. *Advances in computational techniques for structural engineering*, ed. B.H.V. Topping, pp. 99–108, 1996.

[6] Pimenta, P.M. & Campello, E.M.B., Geometrically nonlinear analysis of thin–walled space frames. *Second European Conference On Computational Mechanics*, eds. Z. Waszczyszyn & E. Stein, Cracow, Poland, 2001.

[7] Campello, E.M.B., Pimenta, P.M. & Wriggers, P., A triangular finite shell element based on a fully nonlinear shell formulation. *Computational Mechanics*, **31(6)**, pp. 505–518, 2003.

[8] Pimenta, P.M., Campello, E.M.B. & Wriggers, P., A fully nonlinear multi–parameter shell model with thickness variation and a triangular shell finite element. *Computational Mechanics*, **34(3)**, pp. 181–193, 2004.

[9] Li, S. & Liu, W.K., Meshfree and particle methods and their applications. *Applied Mechanics Reviews*, **55(1)**, pp. 1–34, 2002.

[10] Tiago, C. & Pimenta, P., Geometrically exact analysis of space frames by a meshless method. *ECCOMAS Thematic Conference on Meshless Methods*, eds. V. Leitão, C. Alves & C. Duarte, Lisbon, Portugal, pp.

C44.1–C44.8, 2005.

[11] Tiago, C. & Pimenta, P.M., Geometrically exact analysis of shells by a meshless approach. *Third European Conference on Computational Mechanics – Solids, Structures and Coupled Problems in Engineering*, ed. C.A.M. Soares, Lisbon, Portugal, 2006.

[12] Campello, E.M.B., *Modelos não–lineares de casca em elasticidade e elastoplasticidade com grandes deformações: teoria e implementação em elementos finitos*. Ph.D. thesis, Escola Politécnica da Universidade de São Paulo, São Paulo, Brazil, 2005. (In portuguese).

[13] Campello, E.M.B., Pimenta, P.M. & Wriggers, P., A geometrically–exact finite strain shell model for the analysis of initially curved shells. *Sixth World Congress on Computational Mechanics, in conjunction with the Second Asian-Pacific Congress on Computational Mechanics*, Tsinghua University Press & Springer-Verlag: Beijing, China, 2004.

[14] Pimenta, P.M., *Advanced Solid Mechanics*. Texto do curso de Análise não linear III, Departamento de Estruturas e Fundações, Escola Politécnica da Universidade de São Paulo, 2004.

[15] Tiago, C. & Leitão, V., A aproximação GMLS no contexto do EFG: Aplicação a problemas C^1. *Métodos Computacionais em Engenharia (CD–ROM Proceedings)*, eds. C.A.M. Soares, A.L. Batista, G. Bugeda, M. Casteleiro, J.M. Goicolea, J.A.C. Martins, C.A.B. Pina & H.C. Rodrigues, APMTAC, SEMNI: Laboratório Nacional de Engenharia Civil, Lisbon, Portugal, 2004. (in portuguese).

[16] Tiago, C. & Leitão, V., On the procedures to eliminate shear locking in meshless methods. *ECCOMAS Thematic Conference on Meshless Methods*, eds. V. Leitão, C. Alves & C. Duarte, Lisbon, Portugal, pp. A14.1–A14.8, 2005.

[17] Belytschko, T., Krongauz, Y., Fleming, M., Organ, D. & Liu, W.K.S., Smoothing and accelerated computations in the element free Galerkin method. *Journal of Computational and Applied Mathematics*, **74(1–2)**, pp. 111–126, 1996.

[18] Crisfield, M.A., A fast incremental/iterative solution procedure that handles "snap–through". *Computers & Structures*, **13(1–3)**, pp. 55–62, 1981.

[19] Krysl, P. & Belytschko, T., Analysis of thin shells by the element–free Galerking method. *International Journal of Solids and Structures*, **33(20–22)**, pp. 3057–3080, 1996.

[20] MacNeal, R.H. & Harder, R.L., A proposed standard set of problems to test finite element accuracy. *Finite Elements in Analysis and Design*, **1(1)**, pp. 3–20, 1985.